


In the format provided by the authors and unedited.

Continuum of quantum fluctuations in a three-dimensional $S = 1$ Heisenberg magnet

K. W. Plumb ^{1,2*}, Hitesh J. Changlani², A. Scheie², Shu Zhang², J. W. Krizan³, J. A. Rodriguez-Rivera^{4,5}, Yiming Qiu⁴, B. Winn⁶, R. J. Cava³ and C. L. Broholm^{2,4,7}

¹Department of Physics, Brown University, Providence, RI, USA. ²Institute for Quantum Matter and Department of Physics and Astronomy, The Johns Hopkins University, Baltimore, MD, USA. ³Department of Chemistry, Princeton University, Princeton, NJ, USA. ⁴NIST Center for Neutron Research, National Institute of Standards and Technology, Gaithersburg, MD, USA. ⁵Department of Materials Science and Engineering, University of Maryland, College Park, MD, USA. ⁶NScD Division, Oak Ridge National Laboratory, Oak Ridge, TN, USA. ⁷Quantum Condensed Matter Division, Oak Ridge National Laboratory, Oak Ridge, TN, USA. *e-mail: kemp_plumb@brown.edu

**Supplementary information for: Continuum of quantum
fluctuations in a three-dimensional $S=1$ Heisenberg magnet**

K. W. Plumb,^{1,2} Hitesh J. Changlani,² A. Scheie,² Shu Zhang,² J. W. Krizan,³ J. A. Rodriguez-Rivera,^{4,5} Yiming Qiu,⁴ B. Winn,⁶ R. J. Cava,³ and C. L. Broholm^{2,4,7}

¹*Department of Physics, Brown University, Providence RI, 02902*

²*Institute for Quantum Matter and Department of Physics and Astronomy,
The Johns Hopkins University, Baltimore, MD 21218, USA*

³*Department of Chemistry, Princeton University, Princeton, NJ 08544*

⁴*NIST Center for Neutron Research,
National Institute of Standards and Technology, Gaithersburg, MD 20899, USA*

⁵*Department of Materials Science and Engineering,
University of Maryland, College Park, MD 20742, USA*

⁶*NScD Division, Oak Ridge National Laboratory,
Oak Ridge, Tennessee 37831-6473, USA*

⁷*Quantum Condensed Matter Division, Oak Ridge National Laboratory,
Oak Ridge, Tennessee 37831-6473, USA*

(Dated: August 21, 2018)

SI. DETAILS OF SPECIFIC HEAT ANALYSIS

The total specific heat C_p in $\text{NaCaNi}_2\text{F}_7$ is a superposition of lattice, nuclear, and magnetic contributions. In order to isolated the magnetic component both lattice and nuclear contributions must be estimated and subtracted from the total specific heat.

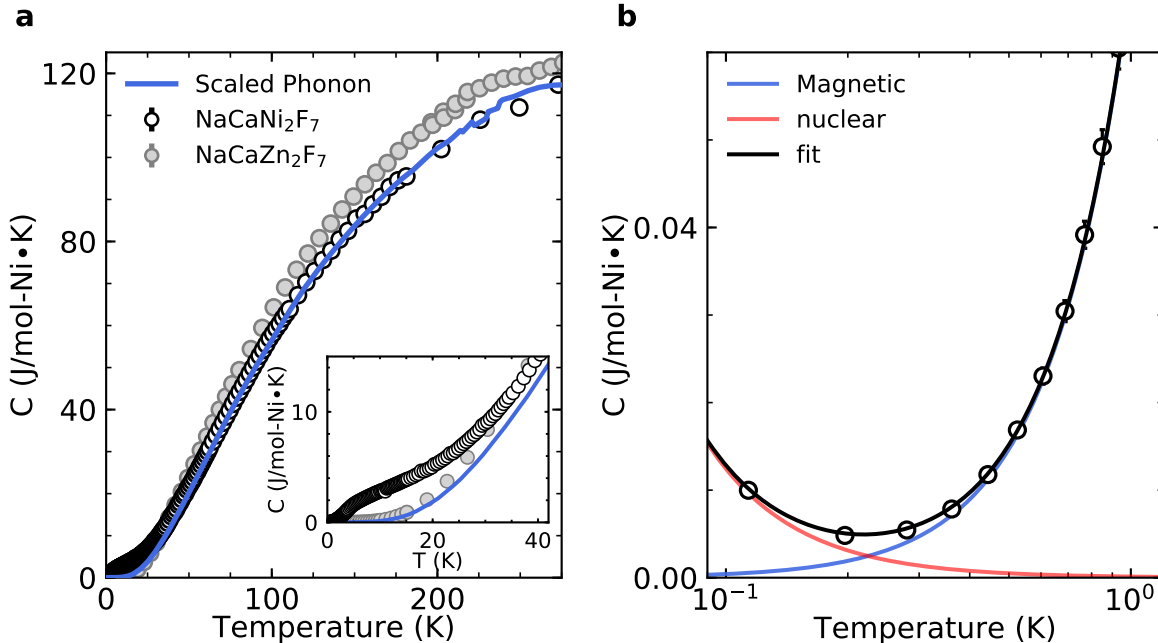


Figure S1: Total specific heat of $\text{NaCaNi}_2\text{F}_7$. **a**, Determination of the phonon contribution. The specific heat of the non-magnetic iso-structural compound $\text{NaCaZn}_2\text{F}_7$ is shown. Solid line is the lattice contribution to C_p for $\text{NaCaNi}_2\text{F}_7$ estimated by scaling the data for $\text{NaCaZn}_2\text{F}_7$ by the relative Debye temperatures of the two compounds. The inset shows details of the low temperature region. **b**, Nuclear and low temperature magnetic contribution.

We first estimated the lattice contribution using a non magnetic iso-structural analog $\text{NaCaZn}_2\text{F}_7$. The total specific heat of both $\text{NaCaNi}_2\text{F}_7$ and $\text{NaCaZn}_2\text{F}_7$, measured between 100 mK and 270 K, are shown in figure S1 a. To model the temperature dependent lattice contributions to C_p in $\text{NaCaNi}_2\text{F}_7$, we scale the specific heat of $\text{NaCaZn}_2\text{F}_7$ by the relative

Debye temperatures of the two compounds which in turn is estimated as follows,

$$\frac{\Theta_{\text{NaCaZn}_2\text{F}_7}^3}{\Theta_{\text{NaCaNi}_2\text{F}_7}^3} = \left(\frac{m_{\text{Na}} + m_{\text{Ca}} + 2m_{\text{Ni}} + 7m_{\text{F}}}{m_{\text{Na}} + m_{\text{Ca}} + 2m_{\text{Zn}} + 7m_{\text{F}}} \right)^{3/2}, \quad (\text{S1})$$

The rescaled phonon specific heat is then given by

$$C_{\text{NaCaNi}_2\text{F}_7}(T) = \frac{\Theta_{\text{NaCaZn}_2\text{F}_7}^3}{\Theta_{\text{NaCaNi}_2\text{F}_7}^3} \cdot C_{\text{NaCaZn}_2\text{F}_7} \left(T \frac{\Theta_{\text{NaCaZn}_2\text{F}_7}}{\Theta_{\text{NaCaNi}_2\text{F}_7}} \cdot T_{\text{NaCaZn}_2\text{F}_7} \right). \quad (\text{S2})$$

The estimated lattice contribution shown as a solid line in figure S1 a was subtracted from C_p to isolate the nuclear and magnetic contributions $C_n + C_m$ shown in figure S1 b. The phonon subtracted low temperature specific heat was then fit between $T = 100$ mK and $T = 2.1$ K using the sum of a nuclear contribution $C_n = \alpha/T^2$ and power law magnetic contribution $C_m = AT^\gamma$, yielding $\alpha = 1.24(5) \times 10^{-4}$ JK/mol, $A = 6.9(3) \times 10^{-2}$, and $\gamma = 2.2(1)$. The magnetic specific heat with phonon and nuclear contributions subtracted is shown in figure 1a of the main text.

SII. SELF CONSISTENT GAUSSIAN APPROXIMATION

In the main text, we obtained parameters of the effective spin Hamiltonian by fitting the energy integrated neutron scattering data to the static structure factor calculated using a self-consistent Gaussian approximation (SCGA). The exchange parameters included in our model Hamiltonian are shown in figure S2.

In this approximation, one relaxes the constraint on the length of individual classical spins and uses the Lagrangian multiplier λ to maintain the global average $\sum_\mu \langle S_i^\mu S_i^\mu \rangle = 1$. The spin configurations are weighted by Boltzmann factor $e^{-\beta\mathcal{H}}$. We take four FCC sublattices (English letter) with three spin components (Greek letter) to form a 12-vector $S_a^\mu(\mathbf{q})$ in the reciprocal space, the corresponding interaction matrix is,

$$\beta\mathcal{H} = \frac{1}{2} \sum_{\mathbf{q}} \sum_{\mu\nu} \{ \beta [J_{ab}^{\mu\nu} 2 \cos(\mathbf{q} \cdot (\mathbf{r}_a - \mathbf{r}_b)) + J_{NNN}^{(2)}(\mathbf{q}) \delta_{\mu\nu}] + \lambda \delta_{ab} \delta_{\mu\nu} \} S_a^\mu(\mathbf{q}) S_b^\nu(-\mathbf{q}), \quad (\text{S3})$$

where \mathbf{q} is the momentum transfer, $J_{ab}^{\mu\nu}$ are the nearest neighbor interactions expressed in global coordinates and $A_{ab}^{(2)}$ is the next nearest neighbor Heisenberg interaction matrix as in Ref. 1. The relaxed constraint now reads,

$$1 = \frac{1}{4N} \sum_{\mathbf{q} \in BZ} \sum_{\alpha} \frac{1}{\beta \epsilon_{\alpha}(\mathbf{q}) + \lambda}, \quad (\text{S4})$$

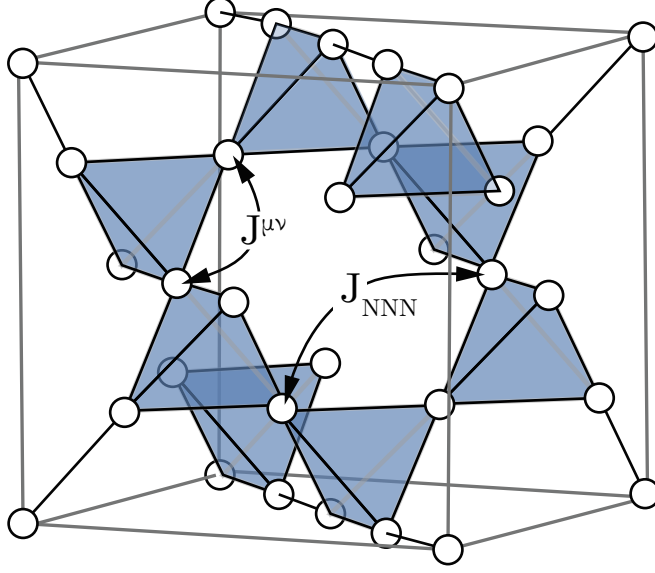


Figure S2: Exchange interactions in the pyrochlore lattice. Only the magnetic Ni sites are shown.

which is solved to obtain λ . Then the spin correlator $G_{ab}^{\mu\nu}$ is calculated as,

$$G_{ab}^{\mu\nu} \equiv \langle S_a^\mu(-\mathbf{q}) S_b^\nu(\mathbf{q}) \rangle = \sum_{\alpha} \frac{[\psi_{\alpha}]_{a,\mu}^{\dagger} [\psi_{\alpha}]_{b,\nu}}{\beta \epsilon_{\alpha}(\mathbf{q}) + \lambda}, \quad (\text{S5})$$

where $\epsilon_{\alpha}(\mathbf{q})$ and ψ_{α} are the eigenvalue and the corresponding eigenvector of the interaction matrix. We sum over the sublattice indices $\sum_{ab} G_{ab}^{\mu\nu}$ to get a tensor with components denoting the spatial directions. The non-polarized neutron cross-section is a sum of all the above correlators with consideration of the appropriate polarization factor,

$$I(\mathbf{q}) = r_0^2 \left| \frac{g}{2} f(q) \right|^2 \sum_{\mu\nu} (\delta_{\mu\nu} - \hat{q}_{\mu} \hat{q}_{\nu}) \langle S_a^\mu(-\mathbf{q}) S_b^\nu(\mathbf{q}) \rangle, \quad (\text{S6})$$

where $r_0 = 0.539 \times 10^{-12}$ cm is the magnetic scattering length, $f(q)$ is the magnetic form factor for Ni^{2+} ,² and g is the isotropic g-factor, $\hat{q}_{\mu}, \hat{q}_{\nu}$ denote unit vectors. To determine the non-spin-flip component of the polarized cross-section we apply a global rotation to $G_{ab}^{\mu\nu}$ to obtain only the components along the guide field direction which was vertical, or perpendicular to the scattering plane. The spin-flip cross-section was then obtained by subtracting the non-spin-flip component from the total magnetic cross-section.

A. Model fitting

The magnetic Hamiltonian was determined through a global χ^2 minimization of equation S6 to the energy integrated neutron intensity. We parameterized the 3×3 interaction matrix $J^{\mu\nu}$ by four independent terms: J_1 , J_2 , J_3 , and J_4 ,³ and include an isotropic next nearest neighbour Heisenberg exchange J_{NNN} . The dipole approximation for the magnetic form factor and $g = 2.28$ ⁴ was used, and we allowed for a small constant background term in the fit. For the vertically focusing neutron spectrometers employed in our measurements the out-of-plane momentum resolution is extremely broad and can qualitatively influence interpretation of the data, even for very diffuse features. We have included the effects of a finite instrumental resolution only along momentum transfers perpendicular to the scattering plane through convolution of of equation S6 with a one-dimensional Gaussian kernel. Optimal parameters were determined utilizing both a basin hopping global minimization routine, and a brute force grid search. Surfaces of χ^2 from the brute force grid search are shown in figure S3.

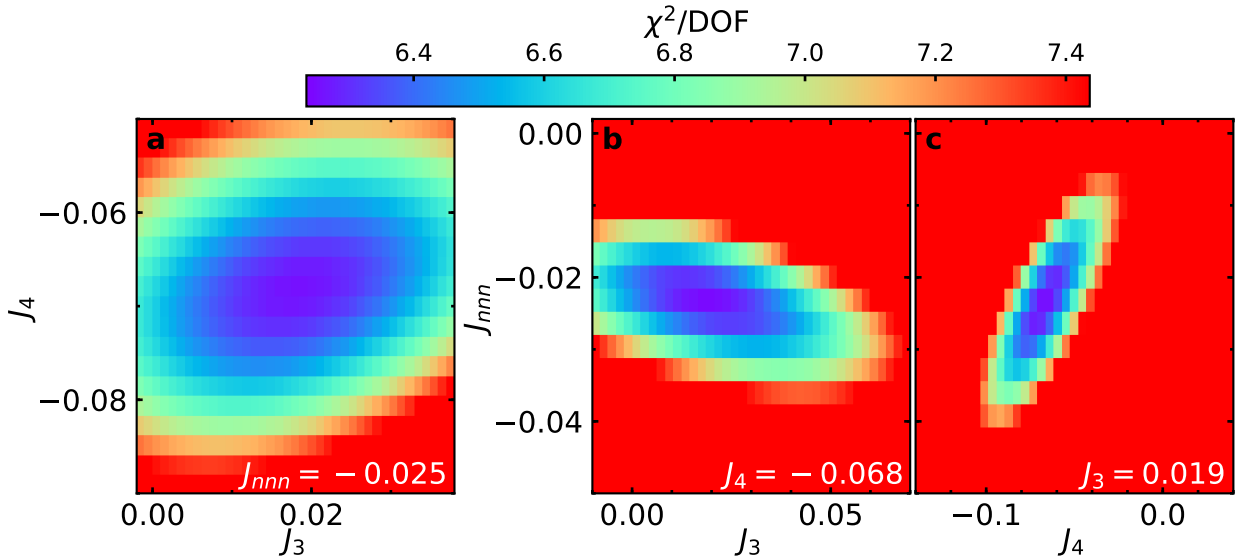


Figure S3: Goodness of fit parameters for SCGA analysis. Surfaces of χ^2 obtained from brute force optimization of the SCGA model with the measured energy integrated neutron intensity at $T = 1.8$ K and with fixed $J_1 = J_2 = 3.2$.

The global minimization constrains $J_1 = J_2$ and the overall sign of these terms. However, we cannot uniquely constrain the magnitude of J_1 using the SCGA alone because this parameter only adjusts an overall intensity scale factor that is correlated with temperature. To provide an initial estimate for J_1 , we use a mean field prediction for the Curie-Weiss temperature which for $J_1 = J_2 \gg (J_3, J_4)$ is $\theta_{CW} \approx -6S(S+1)J_1/3$. The measured Curie-Weiss temperature of $\theta_{CW} = -129$ K gives $J_1 = 3.0$ meV. This was used as a starting parameter to be optimized in the fit along with the other exchange terms, which were initialized with arbitrarily small values. Statistical error bars on the optimized parameters were determined using the bootstrap method, with 100 bootstrap cycles.

Classical Monte Carlo simulations provide a further check. The as determined exchange parameters were input into our Monte Carlo simulations and the results of these simulations compared with the magnetic specific heat as shown in figure 1 (a) of the main text and with the measured static structure factor shown in figure S4.

III. CLASSICAL MONTE CARLO SIMULATIONS

Classical Monte Carlo (MC) calculations were performed on the pyrochlore lattice, its four FCC sublattices with origins at $\mathbf{r}_0 = (1/8, 1/8, 1/8)$, $\mathbf{r}_1 = (1/8, -1/8, -1/8)$, $\mathbf{r}_2 = (-1/8, 1/8, -1/8)$ and $\mathbf{r}_3 = (-1/8, -1/8, 1/8)$, in units of lattice constant a . We consider cubic cells of linear dimension L , a unit cell is made of 16 sites, and thus we work with $N = 16L^3$ lattice sites. Periodic boundary conditions are employed. Disorder, when applicable, was introduced only to the dominant interaction, i.e. the nearest-neighbor Heisenberg term $J = J_1 = J_2$, by assigning to a bond the interaction strength chosen randomly and uniformly from the box distribution $[J - \delta, J + \delta]$ with $\delta = 0.19$ meV. For $L = 8$, with 8192 sites, 50 such disorder realizations were used. The case of $L = 3$, with 432 sites, was also checked using 100 disorder realizations and the conclusions are almost identical.

For comparison to the energy integrated inelastic neutron scattering data at 1.8 K, we performed classical MC simulations at the same temperature with single spin continuous moves with 2×10^6 samples per spin. An additional 10^5 samples per per spin were also used for equilibration. The simulated specific heat (for sizes from $L = 3$ to 10) directly aligns

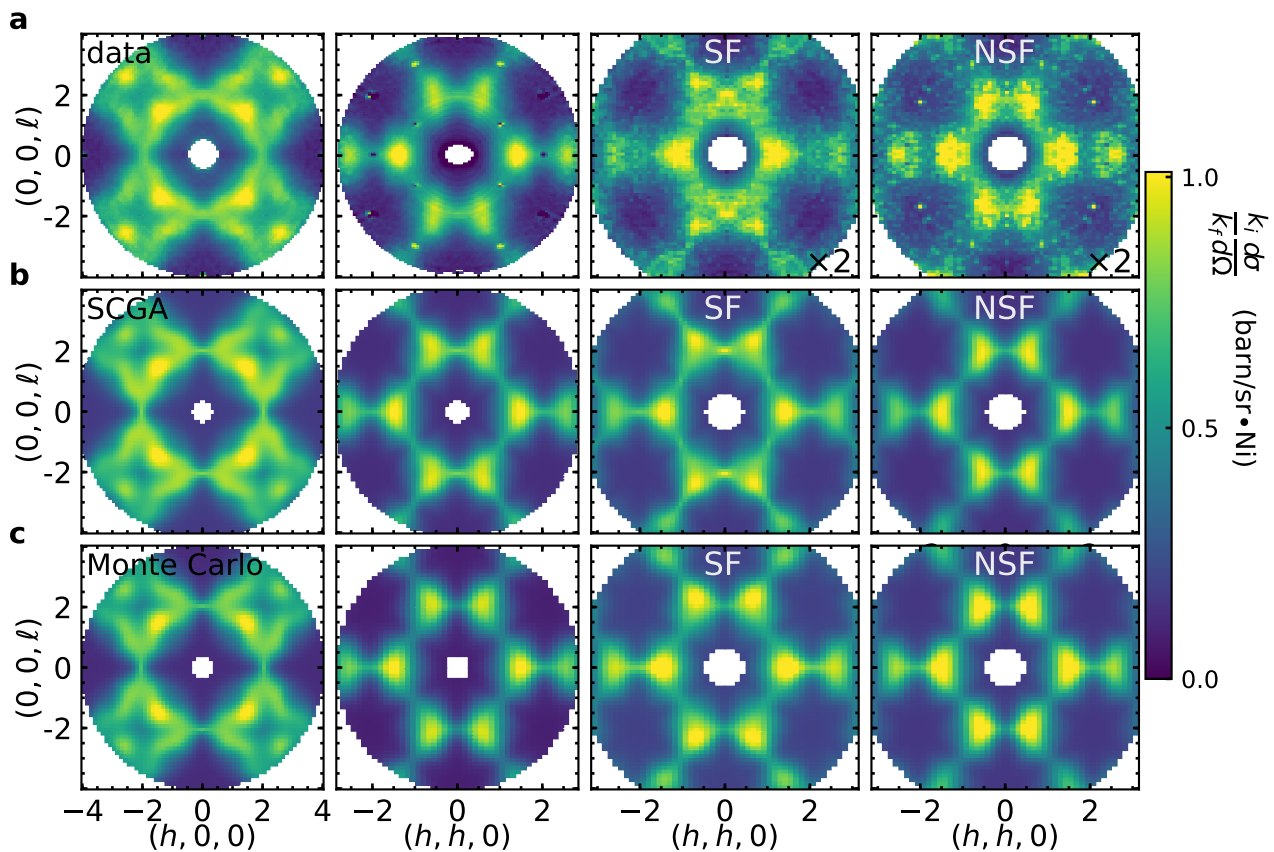


Figure S4: Static structure factor for high symmetry scattering planes from experiment and theory for $\text{NaCaNi}_2\text{F}_7$. NSF and SF are non spin flip and spin flip polarized neutron scattering cross-sections respectively. **a**, Experimental data. **b**, Result of self-consistent Gaussian approximation (SCGA) fit to experimental data. **c**, Classical Monte Carlo simulations used to verify the validity of parameters extracted from the SCGA analysis.

with the measured magnetic specific heat and is presented in Fig. 1 of the main text. The inelastic structure factor for $L = 8$ is presented in Fig. S4 and serves as a cross-check for the SCGA and the Hamiltonian parameters obtained from it.

We also used classical MC in conjunction with parallel tempering moves to obtain the ground, or other low energy, states of the system with and without disorder present. The resulting energy-optimized spin configurations were used to obtain global correlations as

measured by the elastic neutron cross-section and local correlations in the form of two-component order parameters on tetrahedra explained below. The parallel tempering scheme is known to overcome several energy barriers, even in glassy systems and when run sufficiently long can find the ground state. We have employed a unique version of parallel tempering discussed below.

In the parallel tempering scheme, several “replicas” or parallel runs are carried out at sufficiently closely spaced temperatures. Here, we have chosen these temperatures with geometric spacing. The replica number N_r is given by,⁵

$$N_r = \sqrt{N} \ln \left(\frac{T_{max}}{T_{min}} \right) \quad (S7)$$

with T_{min} and T_{max} the minimum and maximum temperatures used. We took $T_{min} = 0.01\text{K}$ and $T_{max} = 1\text{ K}$ and for $L = 8$ chose $N_r = 400$ replicas. A standard single spin move Metropolis algorithm is carried out at each temperature in addition to allowing a replica swap move - configurations at neighboring temperatures are allowed to exchange with a probability in accordance with detailed balance. We allow for replica swap moves after N single site moves. At the end of the MC run with 10^8 moves, the final spin configurations at the 100 lowest temperatures (0.01 K to 0.03 K for $L = 8$) are used as starting points for additional iterative minimization. The latter method has been used in other studies to determine detailed ground state phase diagrams of extended Heisenberg models on the pyrochlore lattice.⁶

In the iterative minimization scheme, each spin experiences the effective field of all the other spins on the lattice. We choose spins at random, and use this local field to determine its optimal direction (the chosen spin wants to anti-align with the local field to minimize the total energy). We typically take the new spin direction to be a combination of the previous spin direction and the optimal direction dictated by the local field.

Once we obtain these low energy configurations, we consider each “building block” of the pyrochlore, say the “up” tetrahedra. For each such tetrahedron, we wish to characterize if the four spins, labeled as $\mathbf{S}_0, \mathbf{S}_1, \mathbf{S}_2, \mathbf{S}_3$, are collinear, coplanar, canted, etc. Instead of directly looking at the real space spin directions, we systematically classify the local order parameter following Ref. 7. This procedure is meaningful under the assumption that all

spin configurations which correspond to low-energy local minima in the energy landscape have similar distributions of local order parameters. We have assumed that nature mimics this minima-finding process, and using this correspondence have disorder and configuration-averaged structure factors obtained from individual low-energy spin configurations without any additional weighting. This latter procedure gives us an estimate of the elastic neutron scattering cross-section shown in Fig. 1c of the main text. It is important to note that this correspondence is limited by the complete absence of quantum effects in our analysis.

As long as the spin configurations approximately lie within the constrained manifold of $\mathbf{S}_{\text{tot}} = \mathbf{S}_0 + \mathbf{S}_1 + \mathbf{S}_2 + \mathbf{S}_3 = 0$, which is the case for the Heisenberg model on the pyrochlore lattice, or with sufficiently small deviations, a convenient way of defining local order parameters is,⁷

$$f_1 = \frac{(\mathbf{S}_0 + \mathbf{S}_1)(\mathbf{S}_2 + \mathbf{S}_3) - 2\mathbf{S}_0 \cdot \mathbf{S}_1 - 2\mathbf{S}_2 \cdot \mathbf{S}_3}{\sqrt{12}} \quad (\text{S8})$$

$$f_2 = \frac{\mathbf{S}_1 \cdot \mathbf{S}_3 + \mathbf{S}_0 \cdot \mathbf{S}_2 - \mathbf{S}_0 \cdot \mathbf{S}_3 - \mathbf{S}_1 \cdot \mathbf{S}_2}{2} \quad (\text{S9})$$

For $L = 8$, data from all 2048 up tetrahedra for 50 different runs/disorder realizations is histogrammed. The $f_1 - f_2$ triangle shows the possibilities of local spin configurations, the vertices correspond to collinear spin configurations, and the midpoints of the triangle edges correspond to pairwise collinear but mutually perpendicular spin configurations. Our results have been shown in Fig. 1e of the main text.

Finally, in Fig. S5, we show the histogram of $(\mathbf{S}_{\text{tot}})^2$ for the Heisenberg and fitted anisotropic models with and without bond disorder. As expected, the Heisenberg only model has no configurations which violate the zero spin constraint, adding disorder and small anisotropies increases the violations, but in all cases the deviations from zero are quite small.

¹ P. H. Conlon and J. T. Chalker, “Absent pinch points and emergent clusters: Further neighbor interactions in the pyrochlore Heisenberg antiferromagnet,” *Phys. Rev. B* **81**, 224413 (2010).

² P. J. Brown, *International Tables for Crystallography*, Vol. C (Springer, Berlin, 2006) Chap. 4.4.5, pp. 454–461.

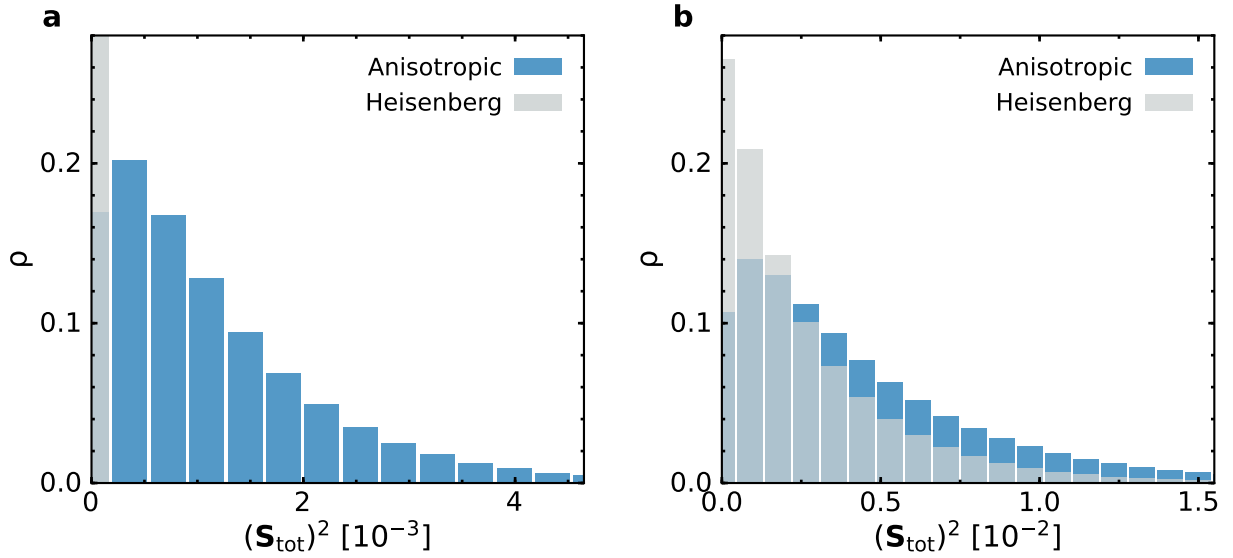


Figure S5: Histogram of $(\mathbf{S}_{\text{tot}})^2$ for Monte Carlo simulations. a With no exchange disorder and with exchange disorder **b**.

³ Kate A. Ross, Lucile Savary, Bruce D. Gaulin, and Leon Balents, “Quantum excitations in quantum spin ice,” *Phys. Rev. X* **1**, 021002 (2011).

⁴ H. Yamaguchi, K. Katsumata, M. Hagiwara, M. Tokunaga, H. L. Liu, A. Zibold, D. B. Tanner, and Y. J. Wang, “Antiferromagnetic resonance in the cubic perovskite KNiF_3 ,” *Phys. Rev. B* **59**, 6021–6023 (1999).

⁵ Koji Hukushima and Koji Nemoto, “Exchange monte carlo method and application to spin glass simulations,” *Journal of the Physical Society of Japan* **65**, 1604–1608 (1996).

⁶ M. F. Lapa and C. L. Henley, “Ground States of the Classical Antiferromagnet on the Pyrochlore Lattice,” ArXiv e-prints (2012), [arXiv:1210.6810 \[cond-mat.str-el\]](https://arxiv.org/abs/1210.6810).

⁷ Oleg Tchernyshyov and Gia-Wei Chern, “Introduction to frustrated magnetism: Materials, experiments, theory,” (Springer Berlin Heidelberg, Berlin, Heidelberg, 2011) Chap. Spin-Lattice Coupling in Frustrated Antiferromagnets, pp. 269–291.